Analytical Methods

Accepted Manuscript

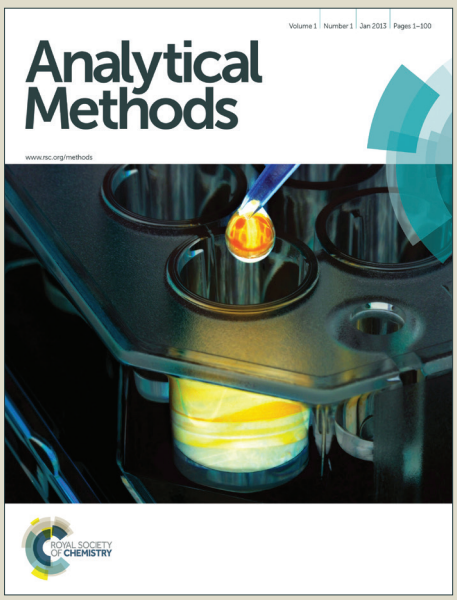

ROYAL SOCIETY OF CHEMISTRY

www.rsc.org/methods

Analytical Methods

RSCPublishing

ARTICLE

Locating microcalcifications in breast histopathology sections using micro CT and XRF mapping

Cite this: DOI: 10.1039/x0xx00000x

Robert Scott,[ab] Catherine Kendall,[a,c] Nicholas Stone,[c] and Keith Rogers[b] ,

Received 00th January 2012,
Accepted 00th January 2012

DOI: 10.1039/x0xx00000x

www.rsc.org/

Spectroscopic measurement of microcalcification chemistry holds great promise as a rapid, quantitative, and non-invasive aid to diagnosis of early stage breast cancer. Previous work has shown that carbonate substitution in hydroxyapatite is highly correlated to breast cancer grade. A deeper understanding of the chemistry-pathology relationships is important in the development of spectroscopic aids to diagnosis. However, investigation of calcification chemistry is hampered by the difficulty of quickly and systematically locating microcalcifications within tissue specimens. We have demonstrated two simple methods based on micro-CT and XRF mapping which can achieve this in sections cut from wax embedded breast tissue from diagnostic archives.

Introduction

Clinical need

Breast cancer is the single biggest cause of cancer deaths in women worldwide,[1] and early detection is critically important in reducing mortality. The principal clinical tool for early detection is mammography, in which a suspicious pattern of radiographically visible calcifications is frequently the earliest diagnostic sign of breast cancer. In one recent study, 76% of ductal carcinoma *in-situ* (DCIS) and 35% of small invasive tumours (< 10 mm) were detected on the basis of calcifications alone.[2] However, the presence of calcifications is common in breast tissue, and mere detection is not sufficient; discrimination is required. At present, the characteristics employed to distinguish suspicious from benign calcifications are based on radiographic appearance, such as size, shape, and distribution. There are well developed rules for incorporation these observations within a risk scoring system, such as BI-RADS. [3] Even so, in the most recent published results from the NHS England screening programme, only 19% women recalled for further investigation following an abnormal mammogram turn out to have cancer. [4] Apart from the cost of these recalls, the psychological distress of a false alarm can be considerable, and women with false--positive mammograms are less likely to return for routine assessment.[5] There is a clear clinical need to improve the positive predictive value of screening.

One proposed addition to the diagnostic armamentarium which may help to achieve this improvement is the use of vibrational spectroscopy to probe the chemistry of calcifications. In particular, the level of carbonate substitution in hydroxyapatite has been shown to be significantly different between benign and malignant calcifications,[6] and this level of substitution decreases with increasing stage and grade of the cancer.[7] Furthermore, it has proved possible to measure differences in the chemical composition of subsurface calcification analogues in tissue, using a range of deep Raman spectroscopy techniques.[8–10] This has the potential to add a new dimension to the characteristics used in diagnosis.

Research on calcification chemistry is not just important for improving diagnostic accuracy. There is emerging evidence that breast cancer cells can play an active role in inducing hydroxyapatite crystallisation, by expression of bone matrix proteins,[11] and conversely that hydroxyapatite crystals in breast tissue can promote mitogenesis, possibly leading to aggravation of tumour growth.[12] Better understanding of calcification chemistry may therefore give valuable insight into the processes of invasion of breast cancer.

Technical challenge

Despite the importance of calcifications in breast cancer detection, and their proposed association with tumour growth, remarkably little detail is known about their chemical composition, or how this relates to pathology. From our own experience, we postulate that one of the reasons for this gap is the difficulty of systematically and precisely locating calcifications for analysis. Many chemical characterisation studies have been based on microspectroscopic analysis of histological sections. This analysis is generally conducted on unstained thin tissue sections, since stains can interfere with the measured spectra, and it is often difficult to identify a calcification definitively from its visual appearance in the absence of staining, particularly from a macroscopic view.

Radiography

The most direct method for locating calcifications within a histological section is to take an X-ray image. Calcifications contained within a thin histological section would be difficult or impossible to locate in this way when mounted on a standard microscope slide or on a typical substrate used for infrared (IR)

spectroscopy, such as a calcium fluoride or barium fluoride window. In principle, it is possible to take an X-ray image of an adjacent histological section mounted on a thin radiolucent substrate such as a polymer film. In order to obtain sufficient contrast in a typical histological section of 3 to 8 µm thickness, it is necessary to use soft X-rays for imaging, ideally just above the calcium k--edge at 4.0 keV. Both mounting on a polymer film and the use of soft X-rays present practical difficulties. In addition, some fragmentation and loss of calcifications can occur on sectioning,[13] which means that some calcifications may be present in the spectroscopic section, but not in the reference radiographic section, or *vice versa*.

Since taking X-ray images of the thin tissue section itself presents some difficulty, another option is to radiograph the whole specimen from which the section is to be cut. This is a useful method for identifying which specimens contain calcifications, prior to sectioning. Radiography of biopsy specimens is routine in clinical practice. However, a single radiograph cannot be relied upon to locate the positions of calcifications in cut sections, since it gives no information on the depth of these within the specimen. Additional radiographic views can help, though overlaps can make correlation of views difficult. A logical extension from taking multiple views is to conduct a CT scan, which can give a complete 3D view of the positions of calcifications in the specimen. The reconstructed volume can be used to determine the expected position of calcifications in the cut sections. This was therefore chosen as one of the methods to explore in this study.

Spectroscopy

An alternative approach is to create a spectroscopic map of entire sections. With many spectroscopic techniques, particularly infrared, mapping multiple samples at sufficient resolution to detect calcifications can be very time consuming. A more suitable technique is X-ray fluorescence (XRF), which can relatively simply create a calcium map. As with X-ray absorption imaging of thin sections, this cannot be conducted on cut sections mounted on a typical substrate used for IR spectroscopy. Calcium fluoride is obviously unsuitable as a substrate for calcium imaging, and barium fluoride gives an excessive background signal which makes detection of the calcium signal difficult. As with CT, a simpler method is to create a map of the block face from which sections are cut. XRF images were taken as part of this study, not only to investigate this as an alternative method, but as corroboration of the presence and position of the CT--detected calcifications.

Coordinate registration

XRF and CT can be used qualitatively to relate calcification position to tissue features. However, in order to relate the positions quantitatively to coordinates within a section, it is necessary to use fiducial markers. Various markers for aligning histological sections in 3-D reconstructions have been proposed since the early 20th century. One of simplest methods consists of small parallel holes drilled through the tissue at right angles to the surface.[14] Various improvements have been suggested such as use of a laser to drill the holes[15] or the use of markers made from such exotic materials as cactus spines[16] and cuttlefish ink[17]. In contrast to most studies on such marker systems, the aim in this case is not to align serial sections, but to register the positions of features in a histological section to an image slice taken through a CT volume or a block face XRF image. Nonetheless, the general requirements identified in earlier work still hold; the markers must be easy to cut, adhere to the slide, and be visible in the required imaging mode.

The situation is simpler with many analyses of calcifications within formalin fixed paraffin embedded (FFPE) breast tissue, since cut sections are frequently not de-waxed. The reason is that calcifications are held in place on the substrate by the wax, and de-waxing can result in their loss. In addition, acquisition of data from tissue embedded in paraffin can reduce the incidence of dispersive artefacts.[18] That means that simple holes in the wax surrounding the tissue can be used as markers, without disturbance to the tissue or the need to introduce foreign materials into the block. That is the approach taken in this study, though other marker systems proposed in the literature could readily be substituted.

Materials and methods

Samples

Formalin Fixed Paraffin Embedded (FFPE) core biopsy breast specimens were selected from the Gloucestershire Hospitals NHS Foundation Trust diagnostic archive, based on the presence of calcifications in the histopathology report. These were screened by mounting the blocks in a Nikon Metrology XT H225 CT system and imaging at 20 kV both perpendicular and parallel to the face of the block. Following screening, 12 blocks were selected with significant levels of calcification at or near the cut surface.

A minimum of three marker holes of Ø0.4 mm were drilled in the selected blocks in a pattern surrounding the tissue. Care was taken to ensure that the hole patterns did not have line or rotational symmetry, to ensure that it was possible to determine unambiguously the orientation of cut sections, and which way up they had been mounted on the slide or substrate.

Two sequential microtome slices of 3 µm were cut from each block and mounted on Ø30 mm x 1 mm barium fluoride discs (Crystran Ltd., Poole) and standard microscope slides respectively. The latter underwent standard haematoxylin and eosin (H&E) processing, and were used for reference.

CT scanning

The FFPE blocks were CT scanned in the Nikon XT H225 system at 30 kV, using 721 projections, and a geometric magnification of 6.0 x, giving a voxel size of 33 µm. The volume was reconstructed using Nikon CT-Pro 3D software.

The reconstructed volumes were then processed using an ImageJ[19] script. This involved cropping and rotating the volume to define the z axis as perpendicular to the cut face and the y axis parallel to the cutting direction, and applying a scale using the calculated voxel size. The first complete image slice from the face of the block was selected and used to determine the position of the calcifications and the fiducial markers. Ellipses were fitted to a thresholded image to determine the marker positions, and the centroid used as the xy position of each hole. The image was then thresholded again to isolate the calcifications, and the centre of the mass of each output to a text file.

X-ray fluorescence imaging

XRF imaging of block faces was conducted using a SII NanoTechnology (now Hitachi) SEA6000VX. Mapping was conducted at 15 kV, with a collimator size of 0.2 x 0.2 mm, collection time of 50 ms per pixel, and at pixel size of 30 - 50 µm. Calcium Kα maps were overlaid on a white light blockface image of the same area captured in the XRF scanner. The machine was freshly calibrated with a test target to ensure x-ray beam and visual image were accurately aligned.

Visible imaging

The list of hole and calcification positions generated by the CT scans was used to determine the expected positions of calcifications on the stage of a Perkin Elmer Spotlight 200 FTIR microscope. The positions of the holes were measured, and the coordinate system of the CT--derived positions transformed to give a least-squares best fit of the holes to their measured positions. This manipulation included scaling coefficients parallel and perpendicular to the cutting direction, as well as rotation and translation. The hole-centre positions under the microscope were determined initially by eye, which enabled the calculated coordinates to be entered directly into the Perkin Elmer Spectrum Image software to drive the stage to the calculated position of the selected calcification. White light transmission maps of the specimens were also analysed to determine the accuracy of the calculated positions.

Results

Qualitative results: A comparison of thresholded CT images and XRF overlay images of typical specimens is shown in Figure 1. It can be seen that there is very good qualitative agreement in the position of calcifications relative to the tissue outlines.

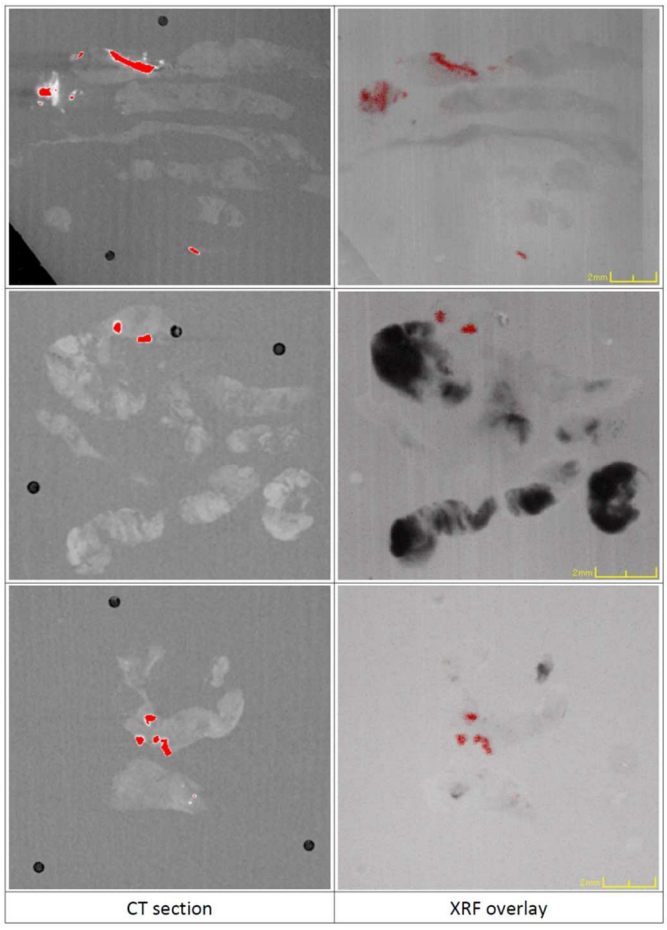

Figure 1: Thresholded CT images and XRF overlay images of three typical FFPE core biopsy breast specimens

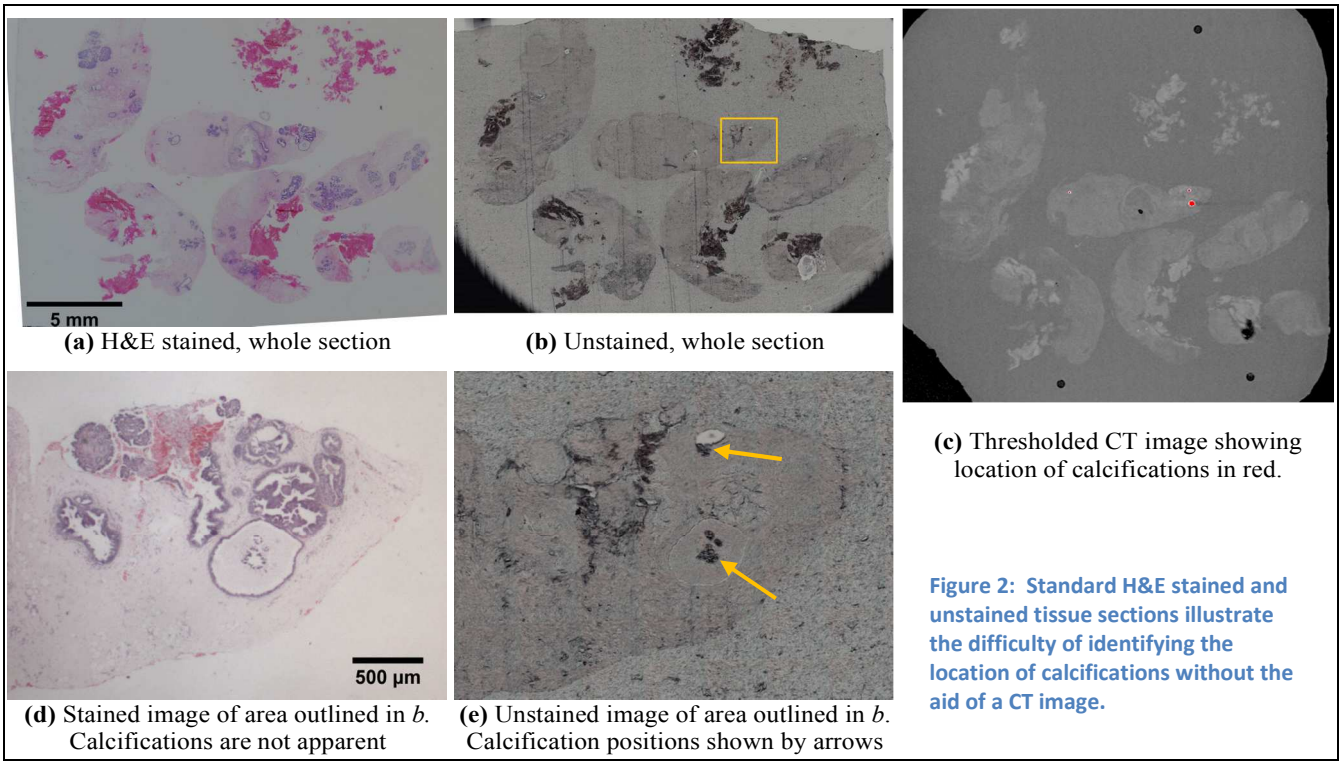

(a) H&E stained, whole section

(b) Unstained, whole section

(c) Thresholded CT image showing location of calcifications in red.

(d) Stained image of area outlined in *b*. Calcifications are not apparent

(e) Unstained image of area outlined in *b*. Calcification positions shown by arrows

Figure 2: Standard H&E stained and unstained tissue sections illustrate the difficulty of identifying the location of calcifications without the aid of a CT image.

The benefits of CT and XRF localisation of calcifications are illustrated in Figure 2. It is not obvious from inspection of either the H&E slide (Fig. 2a) or the unstained tissue (Fig. 2b) whether there are any calcifications present. In contrast the CT image (Fig.2c) at the same magnification clearly shows the location of the calcifications. Comparison with a magnified view of the unstained tissue (Fig. 2e) enables these to be located. Even in this view, it is doubtful that these features could have been definitively identified as calcifications without CT or XRF views. Examination of the same locations on the H&E slide (Fig 2e) shows that in both cases, the calcifications have largely been lost on processing.

Quantitative analysis: The calculated stretching coefficients from the fitting algorithm revealed that the cut sections were all slightly compressed in the cutting direction. The average length change in this direction was -6.7% (95% CI -8.3% to -5.2%). The average change perpendicular to the cutting direction was small and not significant (-0.4%, CI -1.8% to 1.0%). The phenomenon of microtome induced section distortion has been sporadically investigated over many decades, and is reviewed by Jones *et al.*[20] As with the early studies on the subject, compression occurred in the cutting direction.

The transformed best fit hole positions were a median of 0.064 mm from the measured positions (max 0.22 mm). The predicted position of 31 calcifications within the sections was calculated and a comparison made to the centroid of the corresponding calcification as measured from white light transmission images using ImageJ. Calcification centroids were a median distance of 0.12 mm from the location calculated from the hole positions. Typical examples are shown in Figure 3. With five calcifications, this distance exceeded 0.25 mm (max 0.64mm). Four of those were in one specimen, which contained a large linear calcification of approximately 2mm long towards one side of the block, which was disrupted on cutting and may have caused shear distortion of the whole section.

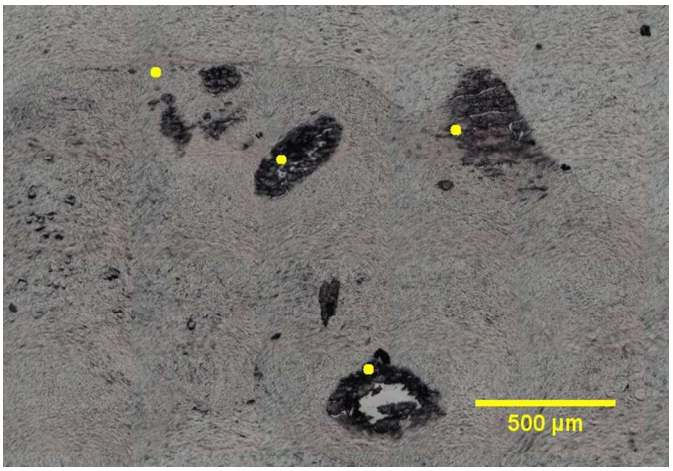

Figure 3 – CT-derived coordinates of four calcifications overlaid on a white light image of an unstained section

Discussion

Both CT scanning of tissue blocks and XRF mapping of the block face proved invaluable for locating calcifications within archive FFPE breast tissue specimens and relating this location to a position on a cut section. In many cases, relating the position visually to the tissue outline is sufficient to locate the calcifications. However, use of fiducial markers has been shown to be capable of providing coordinate locations with sufficient accuracy to locate the calcifications visually, despite distortion of these thin tissue sections.

There are advantages and disadvantages to both methods. In CT images, both tissue outlines and fiducial markers are clearly visible, allowing the spatial relationships to be measured directly. This can be seen in Figure 1. On the other hand, the tissue outline is not directly visible in the XRF maps, requiring an additional step of registering a visible block face image accurately to the XRF map and overlaying the images. However, fiducial markers could in principle be located directly by XRF if they contain sufficient concentration of an XRF detectable element (typically $Z \geq 12$).

Ideally these techniques should measure a thin layer within the specimen which is representative of the microtomed section. With CT, it is possible to select an image slice at an appropriate depth beneath the block surface. Note that even though archive blocks have been trimmed to expose tissue and diagnostic sections previously taken, some facing is still necessary to clean up the surface before the first complete and cohesive sections can be taken. This is typically a few tens of micrometres beneath the surface. Although this CT image slice is thicker than the section thickness (33 µm cf. 3 to 8 µm), it is still substantially smaller than typical dimensions of a microcalcification. XRF derives the calcium signal from a surface layer of the block, the thickness of which depends on the attenuation of the overlying material. The linear attenuation coefficients of calcium Kα radiation (3.7 keV) within breast tissue and cortical bone (a reasonable analogue for breast calcification) are 92 cm^{-1} and 328 cm^{-1} respectively.[21] About 90% of the XRF signal therefore comes from the top 70 µm of a microcalcification, though a 90% attenuated calcium signal may be detected as much as 250 µm below the surface of soft tissue. XRF is therefore in theory more prone than CT to detection of calcified tissue that over-lies or under-lies the cut section, though in practice this did not appear to be a significant problem.

Spatial resolution, sensitivity, and acquisition time for both CT and XRF are an equipment-specific trade-off. In this case, the resolution of the CT was limited by the specimen pixel size of 33 µm. The resolution of the XRF scanner used was limited by the 200 µm minimum collimator size. However, segmentation of closely spaced particles is not a priority in this application, and the resolution of both CT and XRF scanners was adequate for locating individual microcalcifications. Acquisition time for CT in this study was approximately 30 minutes per specimen, though further work has shown that this could be halved with little sacrifice in image quality. Acquisition time for XRF was longer, in the range of 45 to 90 minutes, depending on specimen size; this is more difficult to reduce without an unacceptable reduction in either sensitivity or resolution. With this equipment, CT is a significantly quicker technique.

Conclusions

A systematic and accurate method to identify the location of microcalcifications in breast biopsy histopathology specimens is of great assistance in studying the chemical composition of these clinically important entities. Both the CT and XRF

methods described proved effective of locating calcifications in the surface of wax embedded tissue blocks. Locations could easily be related either to the tissue outline within the wax block or to a coordinate system defined by fiducial markers. These can be matched to locations in microtomed sections, enabling all calcifications present in the section to be studied. Both techniques proved effective, though CT offers some advantages in tissue and marker visibility, depth selectivity, spatial resolution, and speed.

Acknowledgements

We are grateful to Jo Motte and Mark Anniss of the Department of Pathology, Cheltenham General Hospital, for their assistance in identifying and preparing the tissue samples used in this study.

Notes and references

[a] Biophotonics Research Unit, Gloucestershire Royal Hospital, Great Western Road, Gloucester, GL1 3NN, UK.
[b] Cranfield Forensic Institute, Cranfield University, Shrivenham, Swindon, Wiltshire, SN6 8LA, UK.
[c] Biomedical Physics, School of Physics, University of Exeter, Exeter, EX4 4QL, UK.

1. A. Jemal, F. Bray, M. M. Center, J. Ferlay, E. Ward, and D. Forman, *CA. Cancer J. Clin.*, 2011, **61**, 69–90.

2. S. Weigel, T. Decker, E. Korsching, D. Hungermann, W. Böcker, and W. Heindel, *Radiology*, 2010, **255**, 738–45.

3. C. J. D'Orsi, L. W. Bassett, and W. A. Berg, in *Breast Imaging Reporting and Data System: ACR BI-RADS*, eds. C. J. D'Orsi, E. B. Mendelson, and D. M. Ikeda, American College of Radiology, Reston, VA, 4th edn., 2003.

4. J. Patnick, Ed., *NHS Breast Screening Programme Annual Review 2012*, 2012. http://www.cancerscreening.nhs.uk/breastscreen/publications/2012review.html [Accessed 26/11/13]

5. M. Bond, T. Pavey, K. Welch, C. Cooper, R. Garside, S. Dean, and C. J. Hyde, *Evid. Based. Med.*, 2013, **18**, 54–61.

6. A. S. Haka, K. E. Shafer-Peltier, M. Fitzmaurice, J. Crowe, R. R. Dasari, and M. S. Feld, *Cancer Res.*, 2002, **62**, 5375–80.

7. R. Baker, K. D. Rogers, N. Shepherd, and N. Stone, *Br. J. Cancer*, 2010, **103**, 1034–9.

8. R. Baker, P. Matousek, K. L. Ronayne, A. W. Parker, K. Rogers, and N. Stone, *Analyst*, 2007, **132**, 48–53.

9. N. Stone, R. Baker, K. Rogers, A. W. Parker, and P. Matousek, *Analyst*, 2007, **132**, 899–905.

10. P. Matousek and N. Stone, *J. Biomed. Opt.*, 2007, **12**, 024008.

11. R. F. Cox, A. Hernandez-Santana, S. Ramdass, G. McMahon, J. H. Harmey, and M. P. Morgan, *Br. J. Cancer*, 2012, **106**, 525–37.

12. M. P. Morgan, M. M. Cooke, P. A. Christopherson, P. R. Westfall, and G. M. McCarthy, *Mol. Carcinog.*, 2001, **32**, 111–7.

13. J. S. Winston, J. Geradts, D. F. Liu, and P. C. Stomper, *Breast J.*, 2004, **10**, 200–3.

14. A. D. Dixon and P. Howarth, *J. Anat.*, 1958, **92**, 162–6.

15. G. E. Clarke, P. W. Hamilton, and W. A. Montgomery, *Pathol. Res. Pract.*, 1993, **189**, 563–566.

16. M. H. Deverell and W. F. Whimster, *Pathol. Res. Pract.*, 1989, **185**, 602–5.

17. R. Shojaii and A. L. Martel, in *Progress in Biomedical Optics and Imaging - Proceedings of SPIE*, eds. B. M. Dawant and D. R. Haynor, Department of Medical Biophysics, University of Toronto, Toronto, ON, Canada, 2010, vol. 7623, pp. 762331–762331–8.

18. B. Bird, K. Bedrossian, N. Laver, M. Miljković, M. J. Romeo, and M. Diem, *Analyst*, 2009, **134**, 1067–76.

19. C. A. Schneider, W. S. Rasband, and K. W. Eliceiri, *Nat. Methods*, 2012, **9**, 671–675.

20. A. S. Jones, B. K. Milthorpe, and C. R. Howlett, *Cytometry*, 1994, **15**, 95–105.

21. J. H. Hubbell and A. M. Seltzer, *Tables of X-Ray Mass Attenuation Coefficients and Mass Energy-Absorption Coefficients (version 1.4)*., 2004. National Institute of Standards and Technology, Gaithersburg, MD. [Online]: http://physics.nist.gov/xaamdi [Accessed 26/11/13].